Received: 22 February 2023 | Revised: 12 July 2023 | Accepted: 22 July 2023

DOI: 10.1002/qj.4556

RESEARCH ARTICLE

Quarterly Journal of the Royal Meteorological Society RMetS

A balanced model of a hurricane vortex coupled to a boundary layer

Robert J. Beare[1] | **Mike J. P. Cullen**[2]

[1]Department of Mathematics, University of Exeter, Exeter, UK

[2]Retired from Met Office, Exeter, UK

Correspondence
Robert J. Beare, Department of Mathematics, University of Exeter, Exeter EX4 4QF, UK.
Email: r.j.beare@exeter.ac.uk

Funding information
NERC, Grant/Award Number: NE/T003898/1

Abstract

The boundary layer plays a key role in several aspects of hurricane dynamics. Here we focus on its contribution to the balanced circulation. Previous studies, whilst including centrifugal terms, have not included an explicit balance in the boundary layer. Here, we improve the balanced theory to include an Ekman balance, the so-called frictional axisymmetric vortex (FAV). This approach is analogous to semigeostrophic theory that includes realistic boundary-layer diffusion: semigeotriptic (SGT) theory. We formulate the FAV for an axisymmetric system in cylindrical polar coordinates. We then derive a Sawyer–Eliassen equation for the vertical circulation. Example solutions for idealised hurricane-scale and synoptic-scale vortices are compared.

KEYWORDS

balance, centrifugal, Ekman balance, hurricane, synoptic

1 | INTRODUCTION

A hurricane vortex has a significant range of spatial and time scales (Emanuel, 1991). For example, there is the large-scale advective dynamics acting over tens of kilometres, interacting with fast physics such as latent heating and precipitation; there is also the boundary-layer and surface turbulent transfer acting on scales smaller than 1 km. None of these processes can be neglected in weather prediction models, so the challenge is capturing this large range of scales and their interactions through the dynamics and the subgrid parametrizations. Whilst the full range of processes is necessary for prediction, there is benefit from isolating some of these processes to understand the components of these hurricane dynamics. The approach of this article is to focus on the boundary layer's interaction with the large-scale dynamics.

Despite the small horizontal scales of a hurricane, Bui *et al.* (2009) demonstrated that a gradient-balanced approach accounts for a substantial amount of the flow. Also, Smith and Montgomery (2008) emphasised the unbalanced advective flow in the hurricane core in the boundary layer. Ji and Qiao (2023) provide a helpful review of development of the Sawyer–Eliassen equation for hurricane studies from its inception (Eliassen, 1962). For this study, we pick up at the point in history of the balanced approach of Bui *et al.* (2009); here they formulated a Sawyer–Eliassen equation for the circulation in the vertical plane (vertical and horizontal winds) by applying gradient-wind thermal wind balance to the equations of motion. The coefficients of the Sawyer–Eliassen equation lead to a restrictive solvability condition, such that the fields from a mesoscale model needed to be regularized (smoothed) before being used in it. Moreover, Ji and

Abbreviations: FAV, frictional axisymmetric vortex; SGT, semigeotriptic.

Qiao (2023) modify the right-hand side of the equations of Bui *et al.* (2009) to include unbalanced residuals.

In this article, we pursue an alternative approach where the boundary layer is incorporated into the thermal-wind balance and is imposed on the equations of motion from the start, the so-called frictional axisymmetric vortex (FAV). These FAV equations are analogous to the frictional semigeostrophic ones, the so-called semigeotriptic (SGT) equations. The SGT equations are a set of dynamical equations where the Ekman-balanced (geotriptic) winds are used as the prognostic variables instead of the geostrophic momentum in semigeostrophic theory. Previously, in Beare and Cullen (2013), we derived a Sawyer–Eliassen equation in Cartesian coordinates; the Sawyer–Eliassen equation assumed geostrophic balance above the boundary layer and Ekman balance within; the equation also includes advection due to the boundary-layer flow. This approach leads to an improved solvability condition within the boundary layer via increased positive-definiteness of the vertical coefficients. The theoretical approach is also discussed by Beare and Cullen (2012); Beare and Cullen (2016). The full vertically discrete boundary layer is incorporated in the SGT diagnostic described by Cullen (2018); he showed that, if the correct Met Office Unified Model surface flux condition is also used, the boundary-layer structure is reproduced well. Also, the axisymmetric generalisation of semigeostrophic theory is given by Cullen and Sedjro (2015).

Bui *et al.* (2009) make it clear that their definition of balance does not hold in the boundary layer and is a significant limitation of their work. Our approach aims to correct this deficiency by including a proper boundary-layer balance. Here, we aim to modify the axisymmetric equations to include a boundary-layer balance. This approach will thus extend our previous work (Beare and Cullen, 2013) to include the centrifugal terms. We will demonstrate the performance of our approach using idealised vortices with scales in velocity and length of both a hurricane and a synoptic vortex. Comparing the hurricane solutions with the synoptic scales will help identify the benefit of including the new terms.

2 | METHODOLOGY

2.1 | Equations in cylindrical polar coordinates

Most of the mathematical symbols used here are defined in Table 1; other symbols are defined in the text. The governing FAV equations can be viewed as extending

TABLE 1 Symbols used in this article.

Symbol	Meaning
(r, z, t)	Cylindrical polar coordinates and time
(u_e, v_e)	Frictional-gradient wind in radial and azimuthal directions respectively
(u, v, w)	Wind components in radial, azimuthal and vertical directions respectively
$\frac{D}{Dt}$	Substantive derivative $\frac{D}{Dt} = \frac{\partial}{\partial t} + u\frac{\partial}{\partial r} + w\frac{\partial}{\partial z}$
f	Coriolis parameter (constant)
$\phi(r, z, t)$	Geopotential perturbation
$b(r, z, t)$	Buoyancy perturbation
N	Brunt–Väisälä frequency (constant)
$K_m(r, z)$	Boundary-layer vertical momentum diffusivity
$F_b(r, z)$	Buoyancy tendency
$\mathcal{D}(r, z)$	Diffusion operator $\mathcal{D}() = \frac{\partial K_m \partial()}{\partial z^2}$
$\mathcal{D}'(r, z)$	Diffusion operator in circulation equation $\mathcal{D}'() = \frac{\partial^2}{\partial z^2} K_m()$. $\mathcal{D}' \frac{\partial}{\partial z}() = \frac{\partial}{\partial z}\mathcal{D}()$
$\xi(r, z, t)$	Twice the angular velocity $\xi = \frac{2v_e}{r} + f$
$F(r, z, t)$	$F = \frac{v_e}{r} + f$
$\zeta(r, z, t)$	Absolute vorticity $\zeta = f + \frac{1}{r}\frac{\partial(rv_e)}{\partial r} = F + \frac{\partial v_e}{\partial r}$
$\mathcal{F}_u(r, z, t)$, $\mathcal{F}_v(r, z, t)$	Frictional acceleration in radial and azimuthal directions

the semigeotriptic equations (Beare and Cullen, 2013) to cylindrical polar coordinates and including centrifugal terms. The FAV equations are

$$\frac{Du_e}{Dt} - \frac{vv_e}{r} - fv + \frac{\partial\phi}{\partial r} = \mathcal{D}(2u_e - u), \tag{1}$$

$$\frac{Dv_e}{Dt} + \frac{uv_e}{r} + fu = \mathcal{D}(2v_e - v), \tag{2}$$

$$\frac{Db}{Dt} + wN^2 = F_b, \tag{3}$$

$$\frac{\partial\phi}{\partial z} = b, \tag{4}$$

$$\frac{\partial ru}{\partial r} + \frac{\partial rw}{\partial z} = 0, \tag{5}$$

where for simplicity we have assumed unity background density. Setting the substantive derivative to zero gives

$$-\frac{v_e^2}{r} - fv_e + \frac{\partial\phi}{\partial r} = \mathcal{D}u_e = \mathcal{F}_u, \tag{6}$$

$$\frac{v_e u_e}{r} + fu_e = \mathcal{D}v_e = \mathcal{F}_v, \tag{7}$$

the definition of frictional gradient winds (u_e, v_e). Compared with Beare and Cullen (2013), Equations 1 and 2 now include centrifugal terms (second term in each equation); moreover, mass conservation, Equation 5, is appropriate for cylindrical polar coordinates. Equations 1–7 differ from those of Bui *et al.* (2009) and Kepert (2010), and a more recent article by Heng *et al.* (2017), in that balance is applied to the equations (the so-called semigeotriptic assumption) right at the start of the derivation. In the next sections, we will show that this process also allows for both physically realistic energy evolution and a circulation equation with greater solvability. We also acknowledge the approach of of Ji and Qiao (2023), where the right-hand sides of the equations include terms that account for unbalanced residuals.

2.2 | Energetics

Consider the functional form of the Centrifugal terms, second on the left-hand side of Equations 1 and 2, and the frictional terms on the right-hand side; these functional forms are justified by having the correct limit of frictional gradient wind balance (for $u \to u_e$ and $v \to v_e$) and a physically realistic energy evolution. The derivation of the energetic evolution is based on Beare and Cullen (2013), so we give a summary here. Equations 6 and 7 are deducted from Equations 1 and 2 respectively; the resulting radial momentum equation is then multiplied by u_e and azimuthal momentum equation by v_e and the two equations are summed. The centrifugal terms cancel out of the energetics at this stage. The domain-integrated energy ($E_{\rm int}$) is defined as

$$E_{\rm int} = 2\pi \int_0^{H_d} \int_0^{R_d} \left[\frac{1}{2}(u_e^2 + v_e^2) - zb\right] r\, dr\, dz, \tag{8}$$

where the domain's radial and height dimensions are given by R_d and H_d respectively. The time evolution of $E_{\rm int}$ is then

$$\frac{dE_{\rm int}}{dt} = -2\pi \int_0^{H_d} \int_0^{R_d} K_m \left[\left(\frac{\partial u_e}{\partial z}\right)^2 + \left(\frac{\partial v_e}{\partial z}\right)^2\right] r\, dr\, dz, \tag{9}$$

which is negative-definite and thus physically realistic under the action of friction. As discussed by Beare and Cullen (2012) and Beare and Cullen (2013), the form of the friction term on the right-hand side of Equations 1 and 2 is necessary to ensure this physically realistic negative-definite energy relation; any other formulation would not give the correct energy evolution.

2.3 | Idealised setup and solving frictional gradient balance

For our idealised vortex test case, we prescribe the radial pressure gradient as

$$\frac{\partial \phi}{\partial r} = P_{\max} \exp\left(-\frac{z}{H_v}\right) \begin{cases} r/R_v, & \text{if } r \le R_v, \\ R_v^2/r^2, & \text{otherwise}, \end{cases} \tag{10}$$

where R_v and H_v define the size of the vortex in the radial and vertical directions respectively, and $P_{\max}$ is the maximum radial pressure gradient. By changing values of R_v, we will impose either a hurricane or synoptic-scale vortex. When cyclostrophic balance dominates within the vortex radius (as for a hurricane), the azimuthal wind is proportional to $(r\, \partial\phi/\partial r)^{1/2}$ within the vortex radius, that is, proportional to r, the same profile as a Rankine vortex that Holland (1980) showed is a reasonable approximation in a hurricane. We note, though, that there have been more recent updates to the Rankine formula to include quadratic and cubic terms (Kepert and Wang, 2001). The pressure gradient increases linearly from the centre, peaking at $r = R_v$, then decreasing as an inverse quadratic. In the absence of friction, gradient-wind balance is determined by solving a quadratic equation for the azimuthal wind. For transparency and simplicity, we decided to apply a similar solver here. This approach requires the specification of frictional profiles first and then later inferring the diffusion profiles. Typical similarity profiles are used that are zero above the boundary layer and peak in the middle. The profiles are

$$\mathcal{F}_u = \begin{cases} F_{u0}(1 - z/h)^2, & \text{if } z \le h, \\ 0, & \text{otherwise}, \end{cases} \tag{11}$$

$$\mathcal{F}_v = \begin{cases} -A\, \mathcal{F}_{u0}(z/h)(1 - z/h)^2, & \text{if } z \le h, \\ 0, & \text{otherwise}, \end{cases} \tag{12}$$

where the no-slip surface boundary condition on v_e is ensured by

$$F_{u0} = \frac{\partial \phi}{\partial r}(z = 0). \tag{13}$$

The constant A will be defined later in this section. The $\mathcal{F}_v$ profile ensures the radial wind is zero at both the bottom and top of the boundary layer.

The boundary-layer depth takes a functional form that approximates figure 2 of Kepert and Wang (2001). It increases linearly within the vortex centre, remaining constant beyond $r = R_v$,

$$h = h_{max} \begin{cases} r/R_v & \text{if } r \le R_v, \\ 1 & \text{otherwise.} \end{cases} \quad (14)$$

Rearranging Equations 6 and 7 gives

$$v_e^2 + frv_e - r\frac{\partial \phi}{\partial r} + r\mathcal{F}_u = 0, \quad (15)$$

$$u_e = \frac{r\mathcal{F}_v}{v_e + fr}. \quad (16)$$

Taking the positive (cyclonic) root of the quadratic, Equation 15 gives

$$v_e = -\frac{fr}{2} + \left[\left(\frac{fr}{2}\right)^2 + r\left(\frac{\partial \phi}{\partial r} - F_u\right)\right]^{1/2}, \quad (17)$$

which is as the standard gradient-wind formula, but now with a deduction from the pressure gradient to account for friction. For the remaining circulation calculation, we then diagnose diffusion such that

$$\mathcal{D}v_e = \mathcal{F}_v, \quad (18)$$

and, since v_e and $\mathcal{F}_v$ are known, the diffusion operator, $\mathcal{D}$, is inverted to determine K_m. The constant A in Equation 12 controls the inflow angle of the frictional gradient wind. We are guided by the observed inflow angle (Zhang *et al.*, 2011; Zhang and Uhlhorn, 2012) of 22.6°. The value of $A = 0.85$ is thus used.

2.4 | Circulation equation

In this section, we derive an equation for the vertical circulation induced by the combination of boundary-layer friction and heating. Mass continuity, Equation 5, is encapsulated in the stream-function definition

$$(u, w) = \left(-\frac{1}{r}\frac{\partial \psi}{\partial z}, \frac{1}{r}\frac{\partial \psi}{\partial r}\right), \quad (19)$$

where, for comparison purposes, we have used the same sign convention as Bui *et al.* (2009). Taking $\partial/\partial z$ of Equation 6 and substituting from Equation 4 gives

$$\frac{\partial b}{\partial r} = \xi\frac{\partial v_e}{\partial z} + \frac{\partial \mathcal{D}u_e}{\partial z}, \quad (20)$$

the frictional thermal wind balance. Taking the time derivative of Equation 20, assuming that K_m does not vary in time, gives

$$\frac{\partial}{\partial r}\frac{\partial b}{\partial t} = \left(\xi\frac{\partial}{\partial z} + \frac{2}{r}\frac{\partial v_e}{\partial z}\right)\frac{\partial v_e}{\partial t} + \mathcal{D}'\frac{\partial}{\partial z}\left(\frac{\partial u_e}{\partial t}\right). \quad (21)$$

Note the change of diffusion operator from $\mathcal{D}$ and $\mathcal{D}'$ (see Table 2). The time derivatives in Equations 1–3 are substituted into Equation 21. Many of the first-order derivatives in stream function cancel using Equation 20. Scaling analysis indicated that the remaining first-order derivative terms were negligible. Given the axial flow is much greater than the radial flow, we also follow Cullen (1989) and Bannon (1998) by setting $v = v_e$ (the frictional equivalent of the geostrophic momentum approximation of Hoskins, 1975). The resulting diagnostic equation for the stream function is

$$\begin{aligned} &\left[\xi\zeta + \mathcal{D}'^2 + \frac{\partial u_e}{\partial r}\mathcal{D}'\right]\frac{1}{r}\frac{\partial^2 \psi}{\partial z^2} \\ &\quad + N^2\frac{\partial}{\partial r}\left(\frac{1}{r}\frac{\partial \psi}{\partial r}\right) - 2\frac{\partial b}{\partial r}\frac{1}{r}\frac{\partial^2 \psi}{\partial r \partial z} \\ &\quad = -\left[\xi F + \mathcal{D}'^2\right]\frac{\partial u_e}{\partial z} + \frac{\partial \mathcal{F}_b}{\partial r}. \end{aligned} \quad (22)$$

Equation 22 is an elliptic diagnostic equation for stream function; the equation is forced on the right-hand side by friction (first group of terms) and heating (second term). Equation 22 thus allows a useful diagnostic calculation of the response of the dynamics to the physics for an axisymmetric vortex. This circulation equation differs from that in Bui *et al.* (2009); although both approaches apply thermal wind balance, here a set of equations that are rigorously balanced provides the starting point. As a result, there is more positive definiteness in the resulting

TABLE 2 Parameter values used for the hurricane and synoptic cases.

Symbol	Hurricane value	Synoptic value
N	$1.73 \times 10^{-2}\ \mathrm{s}^{-1}$	Same
f	$1 \times 10^{-4}\ \mathrm{s}^{-1}$	Same
R_v	40 km	1000 km
P_{max}	$0.06\ \mathrm{m \cdot s^{-2}}$	$3 \times 10^{-3}\ \mathrm{m \cdot s^{-2}}$
$\mathcal{H}_{max}$	$25\ \mathrm{K \cdot h^{-1}}$	$2\ \mathrm{K \cdot h^{-1}}$
L_H	20 km	1000 km
$\mathcal{H}_{maxbl}$	$12.5\ \mathrm{K \cdot h^{-1}}$	$5\ \mathrm{K \cdot h^{-1}}$
Rossby no., $\max(v_e)/(fR_v)$	11	0.2
h_{max}	1500 m	Same

 Quarterly Journal of the Royal Meteorological Society RMetS

coefficients in Equation 22, namely from the $\mathcal{D}'^2$ terms. The solvability condition for Equation 22 is

$$\left[\xi\zeta + \frac{K_\mathrm{m}^2}{\Delta z^4} + \frac{\partial u_\mathrm{e}}{\partial r}\frac{K_\mathrm{m}}{\Delta z^2}\right] N^2 - \frac{\partial b}{\partial r}^2 > 0, \tag{23}$$

where the magnitude of the diffusion operator, $\mathcal{D}'$, is approximated by the coefficient $K_\mathrm{m}/\Delta z^2$. Within the boundary layer, diffusion coefficients act to make Equation 22 more elliptic. Positive absolute vorticity also acts to make the solution of Equation 22 more positive definite. In fact, when the absolute vorticity is very large and positive, we anticipate that the the stream function will be significantly reduced and thus suppressed in these regions; we refer to this effect as 'vortex shielding'.

It is helpful to compare this with the corresponding Cartesian case described by Beare and Cullen (2013), applying the same scaling assumptions as above, where

$$\left[f\left(f + \frac{\partial v_\mathrm{e}}{\partial x}\right) + \mathcal{D}'^2 + \frac{\partial u_\mathrm{e}}{\partial x}\mathcal{D}'\right]\frac{\partial^2\psi}{\partial z^2} + N^2\frac{\partial^2\psi}{\partial x^2} - 2\frac{\partial b}{\partial x}\frac{\partial^2\psi}{\partial x\partial z}$$
$$= -\left[f^2 + \mathcal{D}'^2\right]\frac{\partial u_\mathrm{e}}{\partial z} + \frac{\partial \mathcal{F}_\mathrm{b}}{\partial x}. \tag{24}$$

Equations 22 and 24 have the same general structure with the change of coordinate from r to x. Equation 22 also has extra $1/r$ terms contained in ξ, ζ, and F that tend to the Cartesian values at small Rossby numbers (as $r \to \infty$, $\xi, \zeta, F \to f$). For this reason, comparing the hurricane and synoptic scales will be helpful in highlighting the role of these terms.

2.5 | Idealised scenarios

In order to highlight the benefits of including centrifugal terms in the FAV formulation, we considered two contrasting horizontal scales and Rossby numbers. We thus prescribe hurricane (large Rossby number) and synoptic-scale (small Rossby number) vortices; the parameters for these cases are given in Table 2. For the hurricane case, these parameters are guided by the observed and modelled cases of Holland (1980) and Bui *et al.* (2009). For each case, we impose a tropospheric heating rate $\mathcal{H}$, emulating that due to latent heating with

$$\mathcal{H} = \begin{cases} \mathcal{H}_\mathrm{max}\cos\left(\pi(r - R_\mathrm{v})/L_\mathrm{H}\right)^2 & \text{if } |r - R_\mathrm{v}| \le L_\mathrm{H}/2 \\ \cos\left(\pi(z - H/2)/H\right)^2 & \text{and } |z - H/2| \le H/2, \\ 0 & \text{otherwise,} \end{cases} \tag{25}$$

where the heating is maximum at the vortex radius R_v and the mid troposphere and H is the depth of the troposphere.

Within the boundary layer, we also include a heating rate

$$\mathcal{H}_\mathrm{bl} = \begin{cases} \mathcal{H}_\mathrm{maxbl}(8z/h)(1 - z/h)^2 & \text{if } z \le h, \\ 0 & \text{otherwise.} \end{cases} \tag{26}$$

3 | RESULTS

3.1 | Balanced hurricane solutions

The frictional gradient winds for the hurricane-scale case are shown in Figure 1a,b. On the one hand, the pressure gradient forces the azimuthal wind to peak at the surface; on the other hand, the boundary layer (below its depth marked by the dashed line) forces the azimuthal wind to zero over its depth. The boundary-layer depth peaks with the maximum azimuthal wind. The radial wind

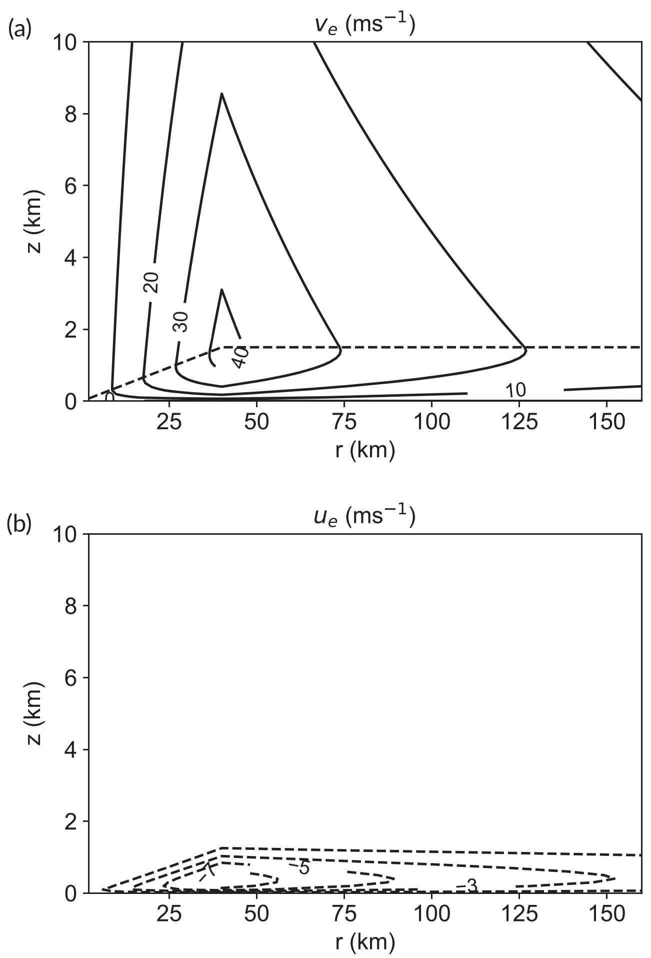

FIGURE 1 (a) Azimuthal frictional gradient wind for hurricane case, solid lines, contour interval 10 m·s^{-1}. Boundary-layer depth is marked by a dashed line. (b) Radial frictional gradient wind, negative values dashed, contour interval 2 m·s^{-1}.

in Figure 1b indicates an Ekman-layer-like wind turning within the boundary layer of order 22.5°, close to the value of 22.6° observed by Zhang and Uhlhorn, 2012.

The maximum azimuthal wind is at r=40 km, with a value of 44 m·s^{-1}, comparable with the observations of developing hurricanes in Holland (1980) and Bui *et al.* (2009). The small radius means that the Rossby number is 11, much larger than one, so the geostrophic wind will be completely inaccurate and the frictional gradient wind and its cyclostrophic limit at small radius are far more physically appropriate. In the cyclostrophic limit, the pressure gradient in Equation 10 equates to just the centrifugal term (v_e^2/r); the azimuthal wind thus varies as r for $r < R_v$.

Figure 2a shows the surface pressure associated with the hurricane vortex; the pressure depth is in agreement with the observational studies of Holland (1980). There is low pressure in the centre and the curvature of the pressure with r varies in a similar way to the observations; integrating Equation 10 with respect to r gives a variation of surface pressure as r^2 for $r < R_v$. Figure 2b shows the potential anomaly in thermal wind balance with the gradient wind, showing a warm anomaly of magnitude 10 K in the vortex centre; this variation follows the friction thermal wind balance, Equation 20, that is, the negative horizontal gradient of buoyancy, balances the negative vertical gradient of geostrophic wind. Since Equation 20 has vorticity as the coefficient of vertical shear, instead of the much smaller Coriolis parameter, this means that the horizontal gradient of buoyancy is greater than the quasigeostrophic formula.

The boundary-layer diffusion is shown in Figure 3a. This follows the imposed boundary-layer depth closely and has a relatively large magnitude due to the large value of the frictional gradient wind, with a maximum close to the surface; the diffusion coefficient is closely correlated to the vertical shear of the azimuthal wind. Figure 3b shows the imposed heating rate, with components that are similar to latent heating (Bui *et al.*, 2009) in the mid troposphere and from the boundary layer. The imposed tropospheric heating models latent heating close to $r = R_v$, as in figure 3 of Bui *et al.* (2009), with a similar magnitude and horizontal distribution above the boundary-layer height.

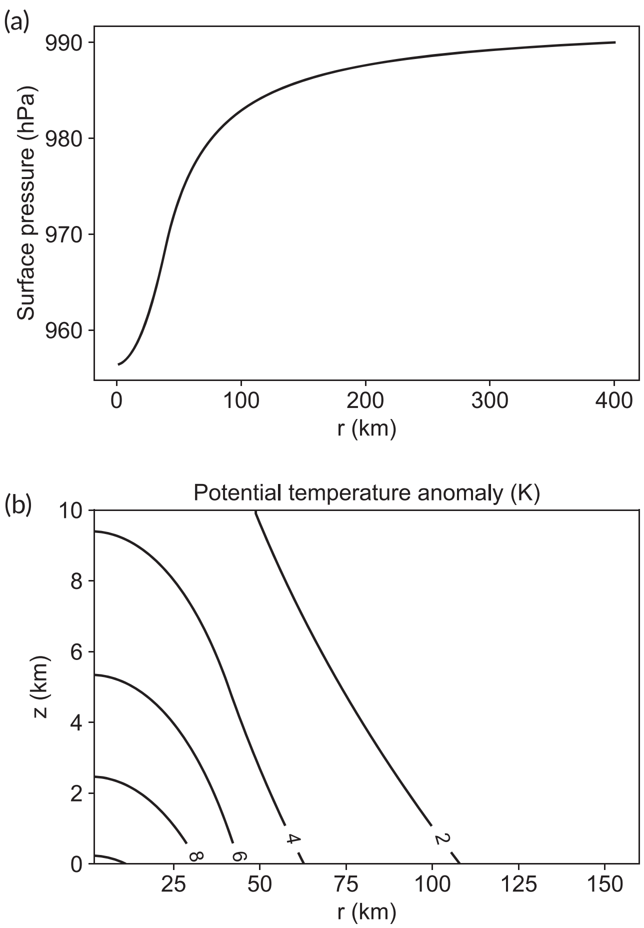

FIGURE 2 (a) Surface pressure with radial coordinate. (b) Potential temperature anomaly, contour interval 2 K.

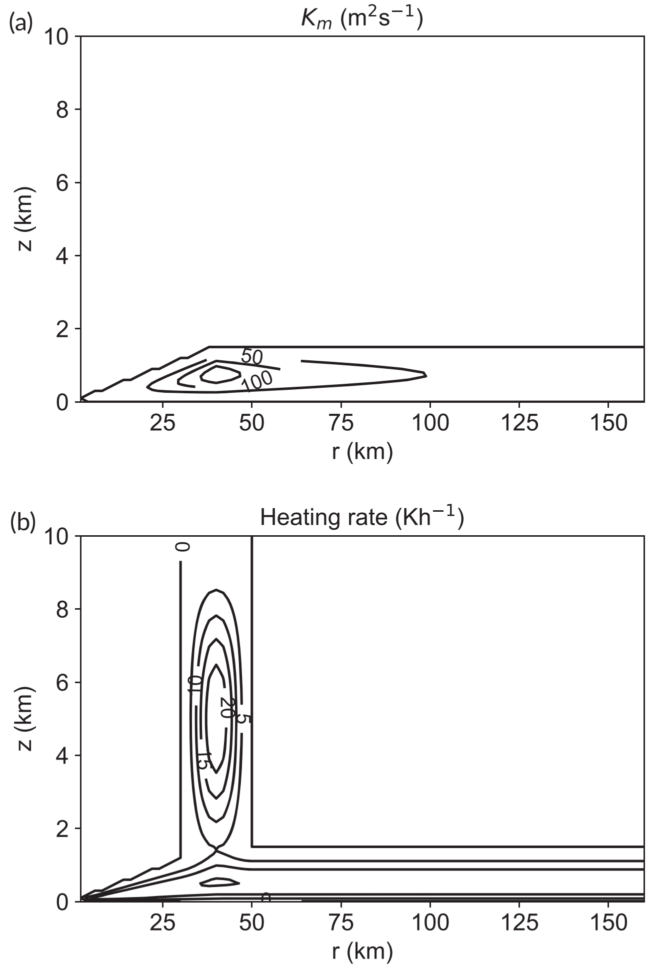

FIGURE 3 (a) Boundary-layer diffusion, contour interval 50 m^2·s^{-1}. (b) Heating rate, contour interval 5 K·h^{-1}.

The boundary layer heating is below the boundary-layer depth and models the heating of a mixed layer below the boundary-layer height.

Figure 4a,b shows the radial and vertical velocity components diagnosed with the Sawyer–Eliassen equation, Equation 22. The inflow velocity (Figure 4a) increases from the right and peaks outside the radius of maximum wind. The decrease of the inflow velocity then converts into an Ekman-pumping-like ascent over the radius of maximum wind; also there is a return radial flow above the boundary layer. This distribution of vertical velocity has more of a low-level boundary-layer component than in Bui *et al.* (2009); comparing Figure 4b with figure 5d of Bui *et al.* (2009), we see similar distributions of vertical velocity, but more vertical velocity low down, due to the imposed boundary-layer balance. This feature is a clear strength of our formulation.

Figure 5a shows the the stream function. The vertical clockwise circulation follows these stream lines, showing both the low-level boundary-layer circulation

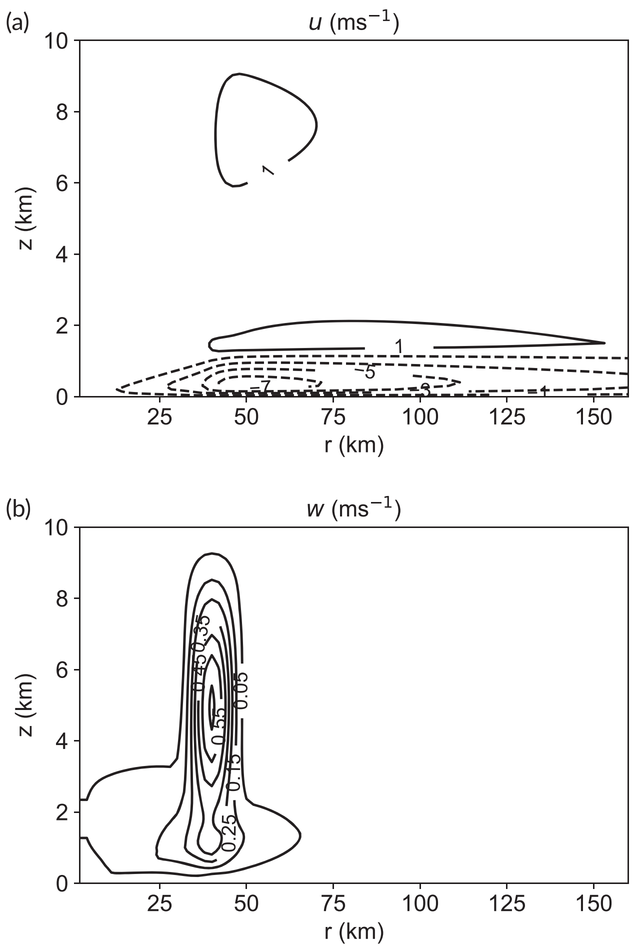

FIGURE 4 (a) Radial velocity diagnosed from Equation 22, contour interval $2\,\mathrm{m\cdot s^{-1}}$, negative values dashed. (b) Vertical velocity diagnosed from Equation 22, contour interval $0.1\,\mathrm{m\cdot s^{-1}}$.

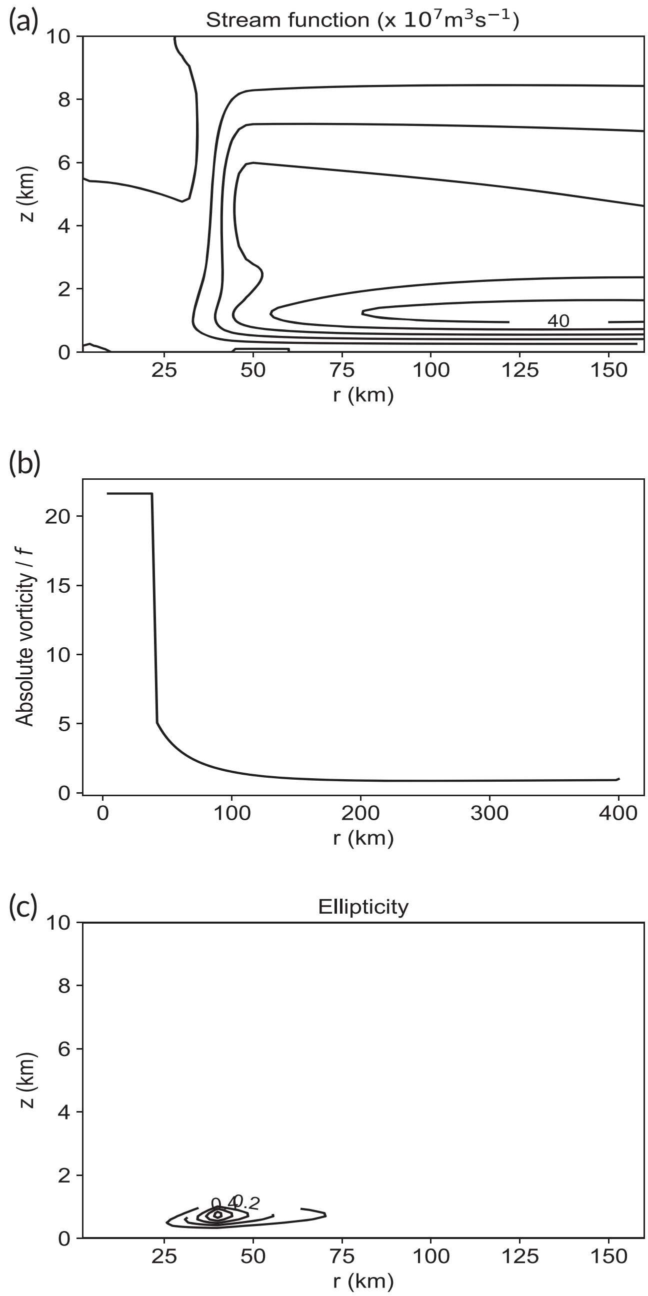

FIGURE 5 (a) Stream function, contour interval $8\times10^{7}\,\mathrm{m^3\cdot s^{-1}}$. (b) Absolute vorticity normalised by f, plotted against r, at height 2500 km. (c) Ellipticity, contour interval $2\times10^{-8}\,\mathrm{s^{-4}}$.

and the mid-troposphere vertical velocity over the radius of maximum wind. Also, the stream function is much smaller within the first 40 km of radius, consistent with the effect of the absolute vorticity in the coefficients of Equation 22 supressing the stream function, or a "vorticity shielding" effect. The positive radial return flow above the boundary layer is consistent with this stream function. The stream-function distribution is also similar to that in figure 4b in Bui *et al.* (2009), but with more vertical gradients within the boundary layer. This effect is illustrated further in Figure 5b, where the absolute vorticity above the boundary layer is much higher within the vortex radius. The high values of relative and absolute vorticity for $r < R_v$ appear in Equations 21 and 22 and reduce the vertical shear of v_e and decrease ψ, respectively, akin to a vorticity shielding effect.

The ellipticity is contoured in Figure 5c, peaking with the boundary-layer diffusion in Figure 3a. In Equation 22, the squared diffusion operator ($\mathcal{D}^2$) is the coefficient of $\partial^2\psi/\partial z^2$, making the solver more positive definite.

3.2 | Contributions from heating and friction

Figure 6 shows another benefit of Equation 22: the ability to split up and associate the contribution of different physical processes to the vertical circulation. Figure 6a shows the vertical velocity due to just the tropospheric heating rate (Equation 25), with values proportional to the heating rate. Figure 6b shows the vertical velocity due to just the boundary-layer drag, an example of the benefit of our formulation; this vertical velocity can be viewed as the analogue of Ekman pumping, but using the frictional gradient balance as the basis. This component is not present in the diagnosis of Bui *et al.* (2009). The horizontal radial wind from the boundary layer converts, via continuity, into a vertical velocity that is maximum at the vortex radius. Finally, Figure 6c shows the contribution from the heating rate in the boundary layer, of much smaller magnitude than the other processes, peaking below the region of maximum boundary-layer depth. Although the boundary-layer heating has a significant magnitude, its horizontal gradient is much smaller, contributing a much smaller component to $\partial F_b/\partial r$ on the right-hand side of the Sawyer–Eliassen equation, Equation 22.

3.3 | Comparison with Cartesian formulation

It is useful to compare our results with the previous Cartesian formulation of Beare and Cullen (2013), as this helps highlight the benefits of including the centrifugal terms here; in the Cartesian case, a geostrophic wind is assumed above the boundary layer, compared with the gradient wind. Figure 7 compares the frictional gradient wind and the frictional geostrophic values. Clearly the geostrophic values are much larger by a factor of 10 and thus unrealistic; this difference is due to the Rossby number being much greater than one within the vortex radius and thus the geostrophic wind being very inaccurate.

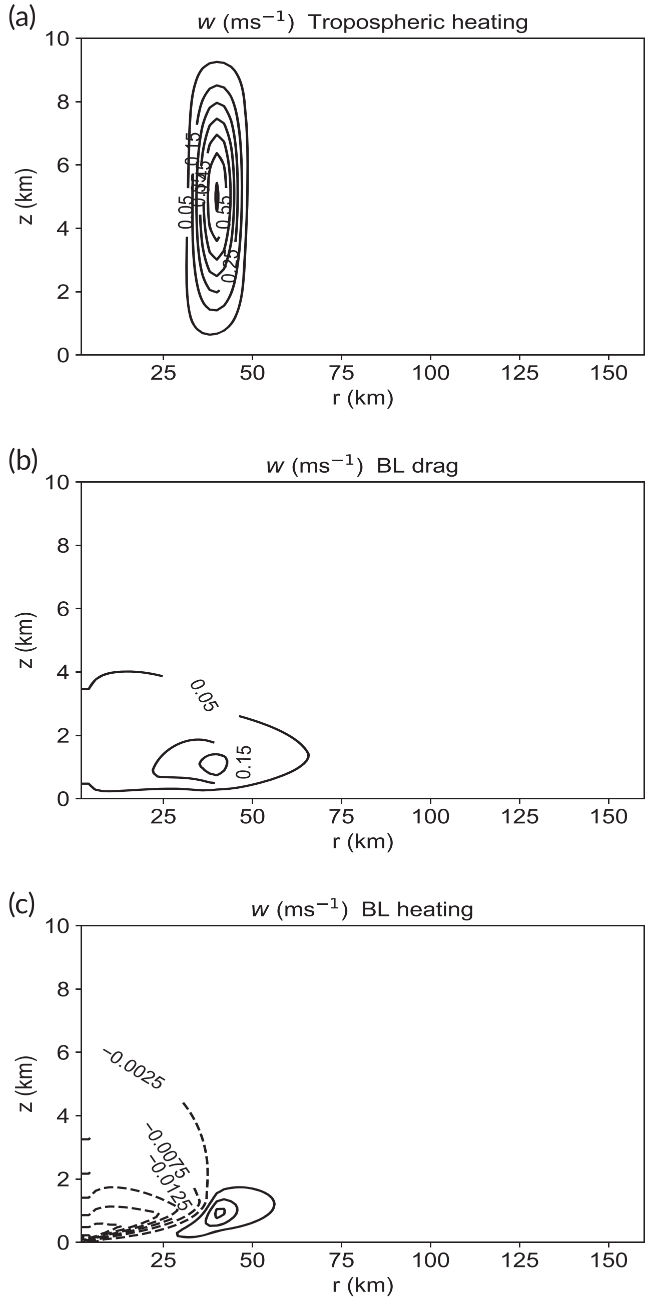

FIGURE 6 (a) Vertical velocity, contour interval 0.1 m·s^{-1}, due to just tropospheric heating. (b) Vertical velocity, contour interval 0.1 m·s^{-1}, due to just boundary-layer drag. (c) Vertical velocity, contour interval 0.005 m·s^{-1}, due to just boundary-layer heating. Note the smaller contour interval.

However, when we increase the radius to synoptic scales (Figure 8), the current formulation and the geostrophic values are a lot closer; this result is consistent with the Rossby number of 0.2 for the synoptic case, compared with the value of 11 for the hurricane scale. This change is further illustrated in the comparison of the vertical velocities from Equations 22 and 24 respectively in Figure 9. The distribution of vertical

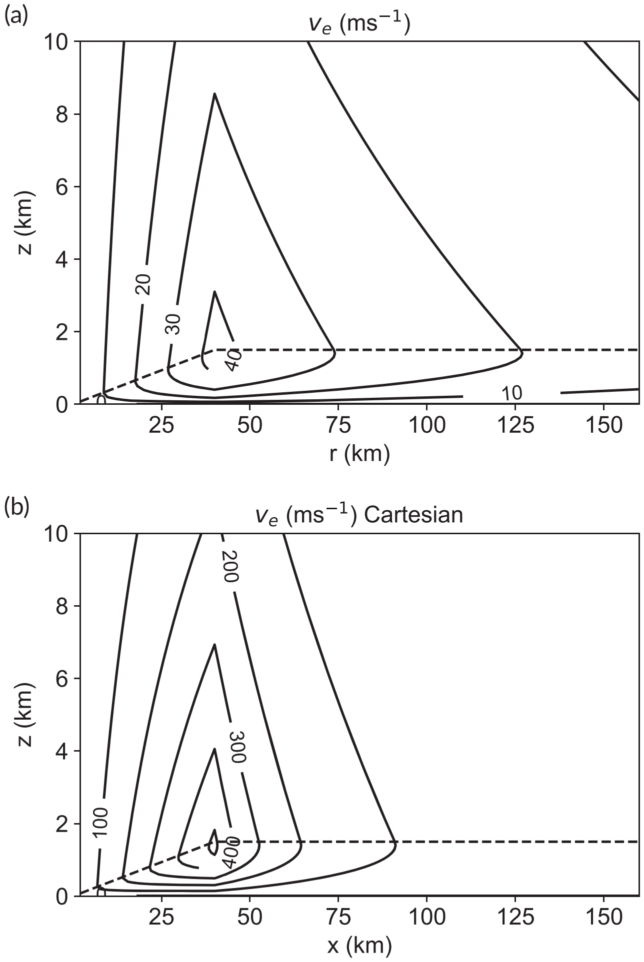

FIGURE 7 A comparison of v_e calculated using (a) frictional gradient balance and (b) the Cartesian (friction geostrophic) balance for the hurricane case. Note the different contour intervals used: 10 m·s^{-1} in (a), 100 m·s^{-1} in (b). Boundary-layer depth is marked by a dashed line.

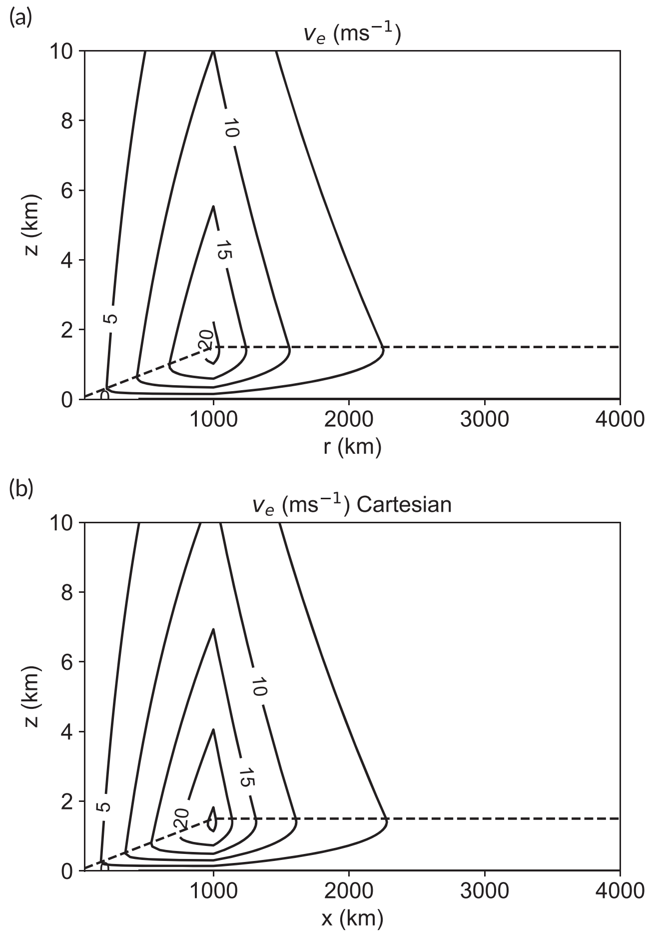

FIGURE 8 Same comparison as Figure 7, but for the synoptic case, contour interval 5 m·s^{-1}.

velocities is very close at the synoptic scale. Thus, the new formulation can be seen as tending to the Cartesian one for large radii. However, even at synoptic scales, the inclusion of the centrifugal correction gives a small improvement in accuracy, as the Rossby number is still finite.

4 | CONCLUSIONS

In this article, we have improved the balanced theory of hurricane dynamics (Bui *et al.*, 2009) by including an explicit boundary-layer balance. The so-called FAV theory is analogous to the Cartesian balanced theory of Beare and Cullen (2013), but now extended to cylindrical polars including the centrifugal terms. As such, the theory is now applicable to a hurricane vortex with large Rossby numbers within the vortex radius. It also adds a next-order improvement to a synoptic-scale vortex. A key result is the improvement of the boundary-layer convergence and low-level ascent. The theory also improves on Bui *et al.* (2009) by introducing extra positive-definiteness to the circulation equation, and thus solvability in the boundary layer.

Whilst we do not claim the theory captures the additional imbalanced flow posited by Smith and Montgomery (2008), it does also include advection within the boundary layer. Others, such as Smith and Vogl (2008) and Kepert (2010), have shown the benefit of idealised treatments in understanding hurricane dynamics. Here we have also shown idealised solutions for our circulation equation. Of course, the same formulation could also be applied to real data.

We demonstrated how the theory permits a split of the flow due to heating and drag components. The maximum ascent was correlated with tropospheric heating, and that due to Ekman pumping also peaked at the radius of maximum wind. We anticipate that this ability to identify the heating and drag contributions to the flow should help identify the subgrid parametrizations

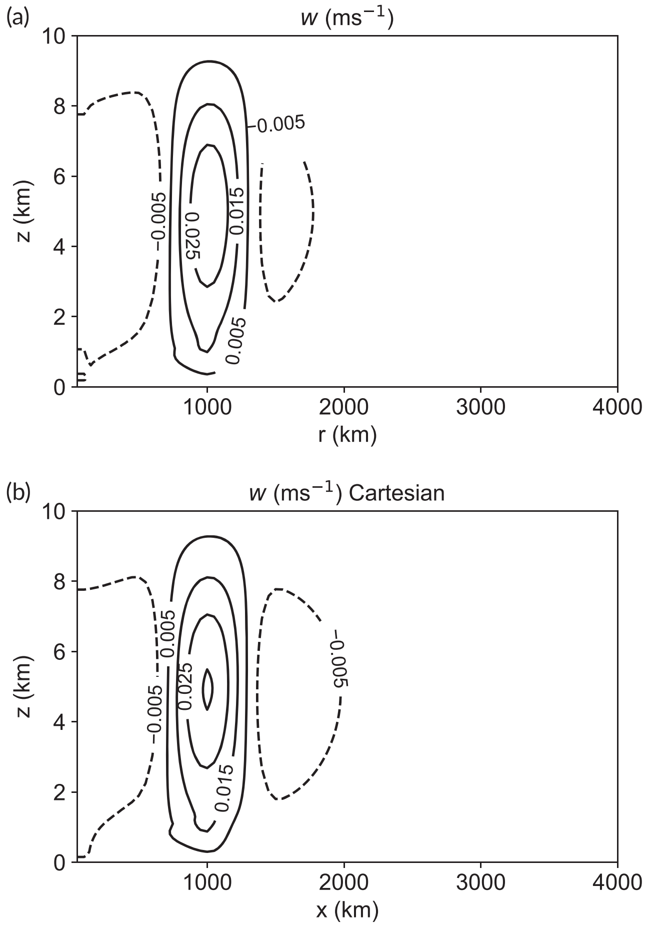

FIGURE 9 Comparison between (a) cylindrical polar and (b) Cartesian diagnosis of vertical velocity for the synoptic case, contour interval 0.01 m·s^{-1}.

responsible in weather prediction models. Not only did the boundary-layer diffusion relax the circulation back to the balanced velocity, but the high absolute vorticity within the hurricane core acted to reduce the stream function and thus deviate the ascent to over the radius of maximum wind.

We now discuss some potential restrictions of our methodology. The calculation of the frictional gradient wind required prescribing drag profiles—this approach provided a way of solving the nonlinear frictional gradient balance for this proof-of-concept study; a more general method might involve combining a vertical solver with the nonlinear solution, so that just a diffusion profile can be prescribed. Whilst the boundary-layer diffusion improves the solvability condition within the boundary layer, a condition similar to that of Bui *et al.* (2009) still applies outside it, so one has to ensure that stratification is sufficiently large outside the boundary layer. In this article, we have demonstrated the FAV theory for idealised hurricane and synoptic vortices with scales motivated by observations. There is still more work to be done with full numerical weather prediction models and beyond the idealised setting here. Although unbalanced motions are still present in real cases (Smith and Montgomery, 2008), the balanced perspective given here provides an invaluable starting point to understanding the flow. Splitting the flow into unbalanced and balanced parts is a valuable perspective.

AUTHOR CONTRIBUTIONS

Robert J. Beare: conceptualization; data curation; formal analysis; funding acquisition; investigation; methodology; software; validation; visualization; writing – original draft; writing – review and editing. **Mike J. P. Cullen:** conceptualization; methodology; writing – review and editing.

ORCID

Robert J. Beare https://orcid.org/0000-0003-0080-655X

REFERENCES

Bannon, P.R. (1998) A comparison of Ekman pumping in approximate models of the accelerating planetary boundary layer. *Journal of the Atmospheric Sciences*, 55, 1446–1451.

Beare, R.J. and Cullen, M.J.P. (2012) Balanced models of boundary-layer convergence. *Quarterly Journal of the Royal Meteorological Society*, 138, 1452–1464.

Beare, R.J. and Cullen, M.J.P. (2013) Diagnosis of boundary-layer circulations. *Philosophical Transactions of the Royal Society A*, 371(20110474), 1–14.

Beare, R.J. and Cullen, M.J.P. (2016) Validating weather and climate models at small Rossby numbers: including a boundary layer. *Quarterly Journal of the Royal Meteorological Society*, 142, 2636–2645.

Bui, H.H., Smith, R.K., Montgomery, M.T. and Peng, J. (2009) Balanced and unbalanced aspects of tropical cyclone intensification. *Quarterly Journal of the Royal Meteorological Society*, 135, 1715–1731.

Cullen, M.J.P. (1989) On the incorporation of atmospheric boundary layer effects into a balanced model. *Quarterly Journal of the Royal Meteorological Society*, 115, 1109–1131.

Cullen, M.J.P. (2018) The use of semigeostrophic theory to diagnose the behaviour of an atmospheric GCM. *Fluids*, 3(72), 1–18.

Cullen, M.J.P. and Sedjro, M. (2015) On a model of forced axisymmetric flows. *SIAM Journal on Mathematical Analysis*, 46, 3983–4013.

Eliassen, A. (1962) On the vertical circulation in frontal zones. *Geophysical Public*, 24, 147–160.

Emanuel, K.A. (1991) The theory of hurricanes. *Annual Review of Fluid Mechanics*, 23, 179–196.

Heng, J., Wang, Y. and Zhou, W. (2017) Revisiting the balanced and unbalanced aspects of tropical cyclone intensification. *Journal of the Atmospheric Sciences*, 74, 2575–2591.

Holland, G.J. (1980) An analytic model of the wind and pressure profiles in hurricanes. *Monthly Weather Review*, 108, 1212–1218.

Hoskins, B.J. (1975) The geostrophic momentum approximation and semi-geostrophic equations. *Journal of the Atmospheric Sciences*, 33, 233–242.

Ji, D. and Qiao, F. (2023) Does extended sawyer–Eliassen equation effectively capture the secondary circulation of a simulated tropical cyclone? *Journal of the Atmospheric Sciences*, 80, 871–888.

Kepert, J.D. (2010) Slab- and height-resolving models of the tropical cyclone boundary layer. Part i: comparing the simulations. *Quarterly Journal of the Royal Meteorological Society*, 136, 1686–1699.

Kepert, J.D. and Wang, Y. (2001) The dynamics of boundary layer jets within the tropical cyclone core. Part ii: nonlinear enhancement. *Journal of the Atmospheric Sciences*, 58, 2485–2501.

Smith, R.K. and Montgomery, M.T. (2008) Balanced boundary layers used in hurricane models. *Quarterly Journal of the Royal Meteorological Society*, 134, 1385–1395.

Smith, R.K. and Vogl, S. (2008) A simple model of the hurricane boundary layer revisited. *Quarterly Journal of the Royal Meteorological Society*, 134, 337–351.

Zhang, J.A., Rogers, R.F., Nolan, D.S. and Marks, F.D. (2011) On the characteristic height scales of the hurricane boundary layer. *Monthly Weather Review*, 139, 2523–2535.

Zhang, J.A. and Uhlhorn, E.W. (2012) Hurricane Sea surface inflow angle and an observation-based parametric model. *Monthly Weather Review*, 140, 3587–3605.

How to cite this article: Beare, R.J. & Cullen, M.J.P. (2023) A balanced model of a hurricane vortex coupled to a boundary layer. *Quarterly Journal of the Royal Meteorological Society*, 1–11. Available from: https://doi.org/10.1002/qj.4556